Equivalent dipole sources to estimate the influence of extracellular myocardial anisotropy in thin-walled cardiac forward models

Vincent Jacquemet[a,b]

[a] *Université de Montréal, Département de Pharmacologie et Physiologie, Institut de Génie Biomédical, Montréal, Canada*
[b] *Hôpital du Sacré-Coeur de Montréal, Centre de Recherche, Montréal, Canada*

Correspondence to:

Vincent Jacquemet
Hôpital du Sacré-Coeur de Montréal
Centre de Recherche
5400 boul. Gouin Ouest
Montreal (Quebec)
Canada H4J 1C5
phone: +1 514 338 2222 ext. 2522
fax: +1 514 338 2694
vincent.jacquemet@umontreal.ca

Published in:

Math. Biosci. (2017), vol 286, pp. 31-38

Abstract

The extracellular domain of the heart is anisotropic, which affects volume conduction and therefore body surface potentials. This paper tests the hypothesis that when wall thickness is sufficiently small (such as in the atria), the effect of extracellular anisotropy can be estimated by modifying local dipole current sources. A formula based on the Gabor-Nelson equivalent dipole and on the reciprocity theorem is derived to compute a linear transformation of the dipole sources that approximates in an isotropic volume conductor the far-field of the actual sources in an anisotropic volume conductor. It involves solving three Poisson equation (once for all). The results obtained in an atrial

model embedded in a boundary-element torso model suggest that when wall thickness is < 3 mm, simulated P waves are weakly altered by extracellular anisotropy during sinus rhythm: an anisotropy ratio of 4:1 typically reduced the longitudinal component of the dipole sources by $< 3\%$, increased the transverse component by $< 5\%$, and increased the transmural component by $\approx 25\%$ (which may be relevant in case of epicardial-endocardial dissociation). Due to uncertainty on experimental conductivity values, it is proposed that atrial extracellular anisotropy may be neglected when computing P waves.

Keywords: electrocardiogram; P wave; atrial electrophysiology; equivalent dipole; Gabor-Nelson theorem; boundary element method.

---

1. Introduction

The forward problem of electrocardiography consists in computing the electric potential on the torso from the bioelectric current sources located within the myocardium. These potentials are affected by the volume conduction properties of the torso. Computer models have been developed to estimate the effects of the conduction inhomogeneities created by the heart, the blood and organs such as the lungs [1–10]. Most of these studies focused on the ventricles or neglected extracellular anisotropy in the atria.

The boundary element method [11] has been proposed and validated for computing the atrial contribution to the ECG [7, 12, 13]. This method can incorporate intracellular anisotropy but is not well adapted for taking into account extracellular anisotropy, so its applicability to the cardiac forward problem relies on the hypothesis that extracellular atrial anisotropy has a limited effect. The same question arises when computing atrial electrograms generated by an anisotropic tissue [14].

Due to the thinness of the atria, the effect of extracellular atrial myocardial anisotropy is expected to be small. The rationale is that, in the Henriquez et al. [15] theoretical model of plane wave propagation in a uniform slab of tissue (see also the subsequent paper by Tranquillo et al. [16]), the influence of myocardial extracellular properties on the potential in the surrounding bath disappears when tissue thickness tends to zero. In a more recent and more realistic simulation study by Keller et al. [10], the influence of cardiac extracellular properties on P wave morphology was found to be less important than that of blood, lungs, and skeletal muscles.

In this paper, we propose an approach for assessing not only the global influence of atrial extracellular anisotropy on the P wave as in previous works, but also for determining the type and location of bioelectric sources that may lead to increased errors, and how the sources could be modified to improve accuracy. The approach is inspired from Potse et al. [9] who adjusted the local dipole current sources in the ventricles in an attempt to reproduce cardiac anisotropy in a boundary-element torso model. Here a theoretical formula is provided to perform the local dipole optimization. The technique is studied as a function of tissue thickness in simplified and more realistic volume conduction models.

2. Methods

2.1. Problem statement

Consider a current-dipole source $\mathbf{d}_0$ located at $\mathbf{x}_0$ within a region Ω (the myocardium) with inhomogeneous and anisotropic conductivity tensor $\boldsymbol{\sigma}(\mathbf{x})$. The rest of the space is assumed to be a uniform and isotropic volume conduction medium with conductivity σ_0. The potential field generated by this dipole at $\mathbf{y}$ in the unbounded (∞) inhomogeneous (i) medium is denoted by $\phi^{i,\infty}(\mathbf{y};\mathbf{d}_0)$. Note that through the application of a transfer matrix to this potential field, body surface potentials in a bounded,

inhomogeneous volume conductor (for instance including lungs and blood cavities) can be derived [11]. Since the volume conduction problem is linear, the field $\phi^{i,\infty}$ can be expressed as $\mathbf{L}(\mathbf{y}, \mathbf{x}_0) \cdot \mathbf{d}_0$. We are seeking a simple, approximate formula for the matrix $\mathbf{L}$.

The problem is to estimate the dipolar moment of an equivalent dipole $\mathbf{d}$ located at the same position $\mathbf{x}_0$ in a uniform (u) isotropic medium with conductivity σ_0 that would generate a potential field, denoted by $\phi^{u,\infty}(\mathbf{y}; \mathbf{d})$, asymptotically similar to $\phi^{i,\infty}(\mathbf{y}; \mathbf{d}_0)$ at large distances $\|\mathbf{y} - \mathbf{x}_0\|$. The objective is to derive a formula to compute $\mathbf{d}$ as a function of $\mathbf{d}_0$, the geometry and volume conduction properties.

2.2. Equivalent dipole estimation

In order to estimate the equivalent dipole, the problem in a bounded medium is first considered. A rectangular parallelepiped P containing Ω is constructed. The volume conduction properties remain the same inside P. The potential field generated by the dipole in the bounded (b) uniform medium and in the bounded inhomogeneous medium are respectively denoted by $\phi^{u,b}(\mathbf{y}; \mathbf{d})$ and $\phi^{i,b}(\mathbf{y}; \mathbf{d}_0)$.

The equivalent dipole may be approximated using the Gabor-Nelson theory [17], according to which the dipole moment is obtained as a surface integral over the outer surface P

$$\mathbf{d} = \sigma_0 \int_P \phi^{i,b}(\mathbf{y}; \mathbf{d}_0)\ \mathbf{n}\, \mathrm{d}S(\mathbf{y})\ , \tag{1}$$

where $\mathbf{n}$ is the normal vector. If the domain Ω was uniform with conductivity σ_0, the integral would give $\mathbf{d} = \mathbf{d}_0$. This approach has been previously used to derive vectorcardiographic transfer matrices [18].

The Green's function $G^{i,b}(\mathbf{y}, \mathbf{x})$ is the potential in the bounded inhomogeneous medium generated at $\mathbf{y}$ by a point source located at $\mathbf{x}$, i.e. $\nabla_{\mathbf{y}} \cdot \boldsymbol{\sigma} \nabla_{\mathbf{y}} G^{i,b}(\mathbf{y}, \mathbf{x}) = -\delta(\mathbf{y} - \mathbf{x})$ with no-flux condition at the boundary of P. Therefore, the field generated

by the dipole $\mathbf{d}_0$ can be written as:

$$\phi^{i,b}(\mathbf{y};\mathbf{d}_0) = \nabla_{\mathbf{x}} G^{i,b}(\mathbf{y},\mathbf{x}_0)\cdot\mathbf{d}_0 \ , \tag{2}$$

where by definition the gradient is a row vector. Combining (1) and (2), the equivalent dipole is estimated as a linear transformation of the real dipole:

$$\mathbf{d} = \left(\sigma_0 \int_P \mathbf{n}\cdot\nabla_{\mathbf{x}_0} G^{i,b}(\mathbf{y},\mathbf{x}_0)\,\mathrm{d}S(\mathbf{y})\right)\cdot\mathbf{d}_0 = M(\mathbf{x}_0)\cdot\mathbf{d}_0, \tag{3}$$

The six faces of P are denoted by P_k^+ and P_k^- for $k=1,2,3$. Then, the matrix M can be expressed as

$$M(\mathbf{x}_0) = \sigma_0 \sum_{k=1}^{3} \mathbf{e}_k\cdot\nabla_{\mathbf{x}_0}\left(\int_{P_k^+} G^{i,b}(\mathbf{y},\mathbf{x}_0)\,\mathrm{d}S - \int_{P_k^-} G^{i,b}(\mathbf{y},\mathbf{x}_0)\,\mathrm{d}S\right) \tag{4}$$

since $\mathbf{n} = \pm\mathbf{e}_k$ on $P_k^\pm$ if $\{\mathbf{e}_k\}$ forms the orthonormal basis associated with the parallelepiped P. After application of the theorem of reciprocity $G^{i,b}(\mathbf{y},\mathbf{x}) = G^{i,b}(\mathbf{x},\mathbf{y})$, the term in parentheses, denoted by $\phi_k^{i,b}$, is written as

$$\phi_k^{i,b}(\mathbf{x}_0) = \int_{P_k^+} G^{i,b}(\mathbf{x}_0,\mathbf{y})\,\mathrm{d}S - \int_{P_k^-} G^{i,b}(\mathbf{x}_0,\mathbf{y})\,\mathrm{d}S \tag{5}$$

and is the solution to the volume conduction equation in the bounded inhomogeneous medium with distributed current source of intensity $+1$ on the face P_k^+ and intensity -1 on the face P_k^-.

The matrix $M(\mathbf{x}_0)$ can therefore be computed for every source location $\mathbf{x}_0$ in Ω by solving three Poisson problems to determine the fields $\phi_k^{i,b}$ and by inserting their gradient in the rows of the matrix M.

Note that if all conductivities are scaled by the same factor κ, then by the definition of the Green's function, $G^{i,b}$ is divided by κ while σ_0 is multiplied by κ, which means that the matrix M is invariant to such scaling (based on Eq. (4)).

If a sufficiently large parallelepiped P is used, the matrix M does not depend on P because $\phi_k^{i,b}(\mathbf{x})$ converges in Ω. Also, when P becomes large, $\phi^{i,b} \to \phi^{i,\infty}$ and $\phi^{u,b} \to \phi^{u,\infty}$ so that $\mathbf{d} = M(\mathbf{x}_0)\mathbf{d}_0$ provides a solution to the unbounded problem. As a result, an approximation for the far-field generated by a dipole $\mathbf{d}_0$ located at $\mathbf{x}_0$ in an inhomogeneous anisotropic medium is obtained as:

$$\phi^{i,\infty}(\mathbf{y}; \mathbf{d}_0) \approx \phi^{u,\infty}(\mathbf{y}; M(\mathbf{x}_0)\mathbf{d}_0) = \frac{(\mathbf{y} - \mathbf{x}_0)^T M(\mathbf{x}_0)\mathbf{d}_0}{4\pi\sigma_0 \|\mathbf{y} - \mathbf{x}_0\|^3} \ . \tag{6}$$

The entries of the matrix M are non-dimensional and will be called correction factors. These components will be expressed in the local coordinate system associated with fiber orientation.

2.3. Tissue models

The approach was tested in 2D and 3D geometries in which tissue thickness was varied.

The first geometry was an annulus in 2D with a radius of 16 mm (mean of inner and outer radii) and a thickness between 1.5 and 10 mm. The annulus was embedded in a 50 by 50 mm conductive square region (the domain P). Fiber orientation was assumed to be tangent to the circles, so there were three extracellular conductivities: the radial conductivity σ_r, the tangential conductivity σ_θ, and the conductivity of the surrounding bath σ_0 (isotropic). Note that the non-dimensional matrix M depends only on the ratios σ_r/σ_0 and σ_θ/σ_0. To compute far-field potentials, the surrounding bath was then extended to 100 by 100 mm.

The second geometry was based on a 3D atrial model [13] in which atrial wall thickness δ was uniform and varied between 1.5 and 4 mm. For that purpose, the mid-atrial surface was extracted from the original model and the nodes within a distance of $\delta/2$ from the surface were included in the new geometry. Fast conducting bundles

(including the pectinate muscles) were kept intact. The atria were embedded in a parallelepiped P that left at least 5 mm space between the epicardial surface and the boundary. To check convergence, the volume was extended by 5 mm on all six sides. Fiber orientation was assumed to be the same across atrial wall thickness. There were three extracellular conductivities: longitudinal (σ_l) and transverse (σ_t) conductivity, and that of the surrounding bath (σ_0).

The Poisson equation was discretized using a finite differences method [19] on a regular grid with 0.33-mm inter-node spacing. The linear systems were solved using a biconjugate gradient stabilized method with an incomplete LU preconditioner.

2.4. ECG computation

To evaluate the influence of atrial extracellular anisotropy on body surface potentials, P waves were computed. Sinus rhythm was simulated in the monodomain framework using the original atrial model [20] which has a thickness of about 1.6–1.8 mm. The parameters were exactly the same as in [13]. Briefly, the membrane kinetics was described by the Courtemanche model with the conductance of the L-type calcium current g_{CaL} reduced by 50%. The baseline intracellular tissue conductivity was set to 9 mS/cm (longitudinal) and 3 mS/cm (transverse) in the working myocardium. The longitudinal conductivity was increased to 12 mS/cm in the fast conducting system [13]. Normal propagation was initiated by injecting intracellular current in the region of the sino-atrial node.

For the simulation of atrial fibrillation, g_{CaL} was further reduced to 20% of its original value in the left atrium, thus creating a left-right gradient in refractoriness. Longitudinal and transverse intracellular conductivities were reduced to 4 mS/cm and 1 mS/cm. Fibrillatory activity was induced by creating a customized initial condition with two functional reentries, one in the pulmonary vein region and one in the right

atrium free wall [13].

The current sources for the volume conduction problem were given by $\mathbf{d}_0(\mathbf{x},t) = -\boldsymbol{\sigma}_m(\mathbf{x})\,\nabla V_m(\mathbf{x},t)$ where V_m is the membrane potential and $\boldsymbol{\sigma}_m$ is the equivalent conductivity tensor used in the monodomain equation [11]. From the field $\phi^{i,\infty}$ generated by the atria in an unbounded medium (Eq. (6)), body surface potentials in an inhomogeneous torso including lungs and blood cavities were computed using the boundary element method [13].

3. Results

3.1. Two-dimensional test case

The volume conduction problem was first solved in the anisotropic annulus. The extracellular conductivity within the annulus was $\sigma_\theta = 2$ mS/cm (tangent to the annulus) and $\sigma_r = 0.5$ mS/cm (in the radial direction). The surrounding bath was isotropic with a conductivity of $\sigma_0 = 1$ mS/cm. The results only depend on the ratios $\sigma_\theta/\sigma_0 = \sigma_0/\sigma_r = 2$, which were voluntarily slightly more anisotropic than in [9] and within the broad experimental ranges reported in [10].

The matrix $M(\mathbf{x}_0)$, for any $\mathbf{x}_0$ in the annulus, was computed in the local polar coordinate system (r,θ) for a radius of 16 mm and a thickness of 8 and 3 mm. Figure 1 shows the map of the components $M_{\theta\theta}$ and M_{rr}. The mixed components $M_{\theta r}$ and $M_{r\theta}$ were close to zero (mean $< 10^{-12}$ and standard deviation < 0.02). This means that in order to best reproduce the field of a tangent dipole in an inhomogeneous medium using the field generated by a dipole in a uniform medium, the dipolar moment had to be multiplied by a correction factor of 0.916 ± 0.028 (3-mm thickness) or 0.812 ± 0.096 (8-mm thickness).

The correction factor was relatively uniform in the thin-walled annulus (Fig. 1A). In the thicker-walled version (Fig. 1B), the correction factor was smaller in the inner

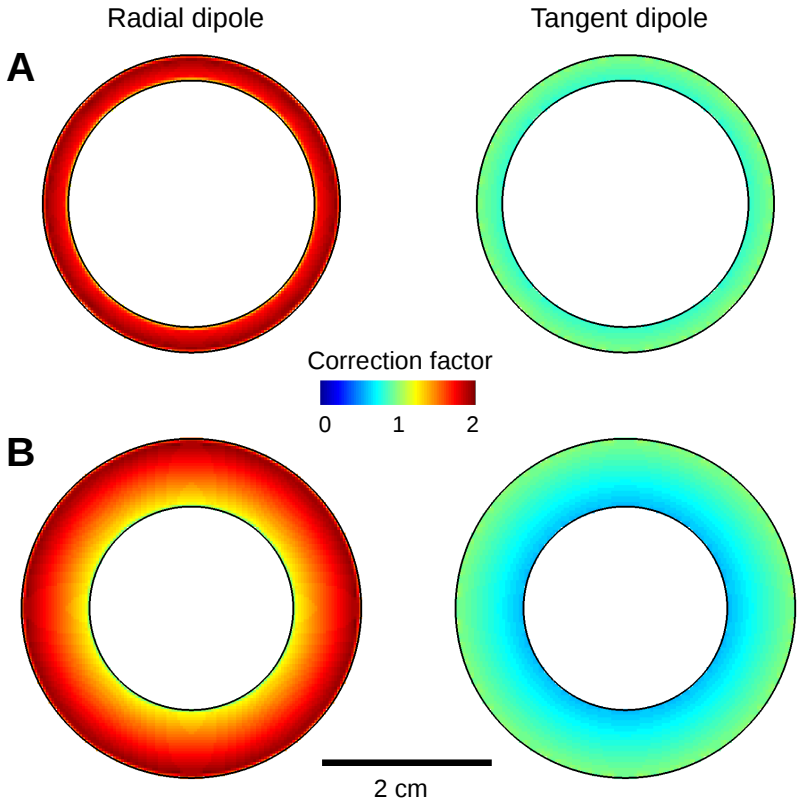

Figure 1: Correction factors M_{rr} (left panels) and $M_{\theta\theta}$ (right panels) for an annulus with a thickness of 3 mm (A) and 8 mm (B).

side (endocardium). To study the effect of wall thickness, the correction factors for tangential and radial dipole was computed as a function of annulus thickness (Fig. 2). As the thickness tends to zero, the correction factors are more uniform throughout the tissue and $M_{\theta\theta}$ tends to 1 and M_{rr} to 2. This means that in very thin layers of tissue, local extracellular anisotropy has little effect on tangential dipole. For radial dipoles, however, the dipolar moment has to be multiplied by $\sigma_0/\sigma_r = 2$.

The results are valid in the limit where the surrounding medium (P) is a box of sufficiently large size. To determine what size is necessary to compute the correction

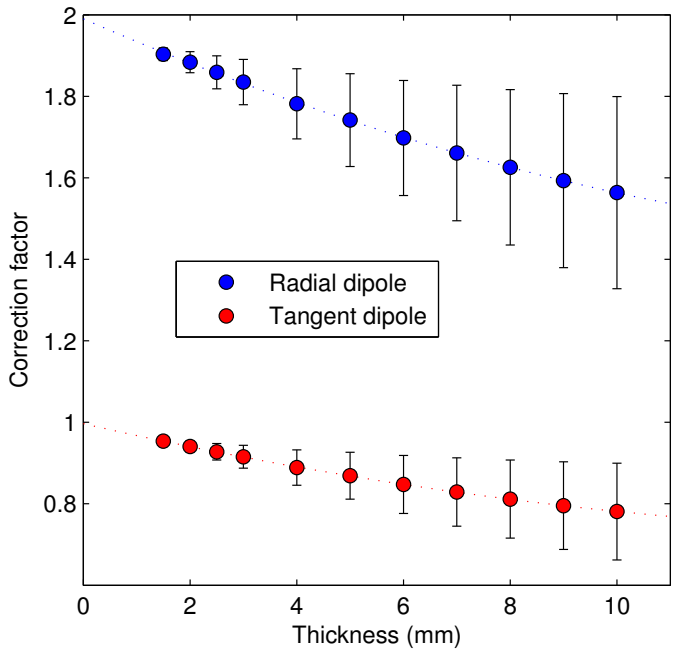

Figure 2: Correction factors M_{rr} (radial) and $M_{\theta\theta}$ (tangent) for annuli of varying thicknesses. The mean and standard deviation of the correction factors over the whole annulus are shown as error bars.

factors, the closest distance between the boundary and the tissue was varied between 1 mm and 50 mm for an annulus of radius 16 mm and thickness 2, 3 and 8 mm. The side length of the square therefore ranged from 36 to 140 mm. The largest square was taken as reference. The relative error was defined as the norm of the difference of all correction factors within the annulus divided by the norm of all reference correction factors. Figure 3 shows that that the box does not need to be large. Simply adding 5 mm around the tissue in all dimensions led to an error $< 0.2\%$. Note that the solution to our Poisson problems is a linear current flow, from one side of the box to the opposite side, that is moderately affected by the presence of a conduction heterogeneity.

Figure 4 shows examples of fields generated in the inhomogeneous (left panels)

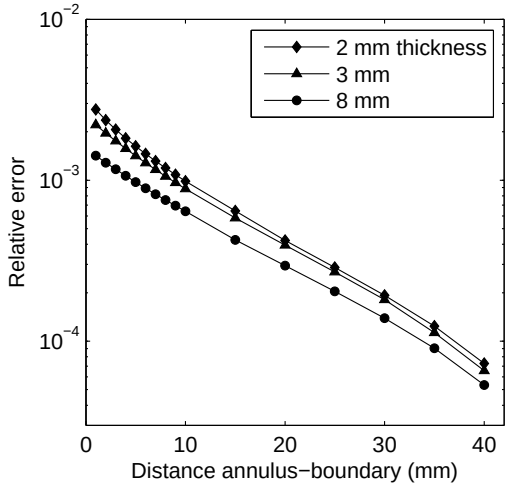

Figure 3: Effect of the size of the surrounding medium (the box P) on the accuracy of the results. The relative error on the correction factors is displayed as a function of the minimum distance between the boundary of the box and the annulus (radius: 16 mm; thickness: 2, 3 and 8 mm).

and in the uniform medium (right panels). When the annulus was thick (8 mm, top panels), the local field (inside the annulus) was significantly different, but the far field was reasonably reproduced by the equivalent dipole (correlation coefficient for values on the boundary: 0.998; relative error on the norm: 9.9%). When the annulus was thin (2 mm, bottom panels), the fields were very similar after application of the correction factor (correlation coefficient: 0.9999; relative error: 1.6%).

The extracellular conductivity within the cardiac muscle may itself be inhomogeneous. An annulus with a thickness of 3 mm was created (Fig. 5A). The annulus was divided into two equal parts. The conductivity was $\sigma_\theta = 1.5$ mS/cm and $\sigma_r = 0.375$ mS/cm in the upper half, and $\sigma_\theta = 2$ mS/cm and $\sigma_r = 0.5$ mS/cm in the lower half. The radial correction factors were 2.26 ± 0.26 in the upper half and 1.76 ± 0.17 in the lower half (Fig. 5A). The tangent correction factors were slightly below 1, as in Fig. 2. The field generated by a radial dipole in each of the halves in the inhomogeneous volume

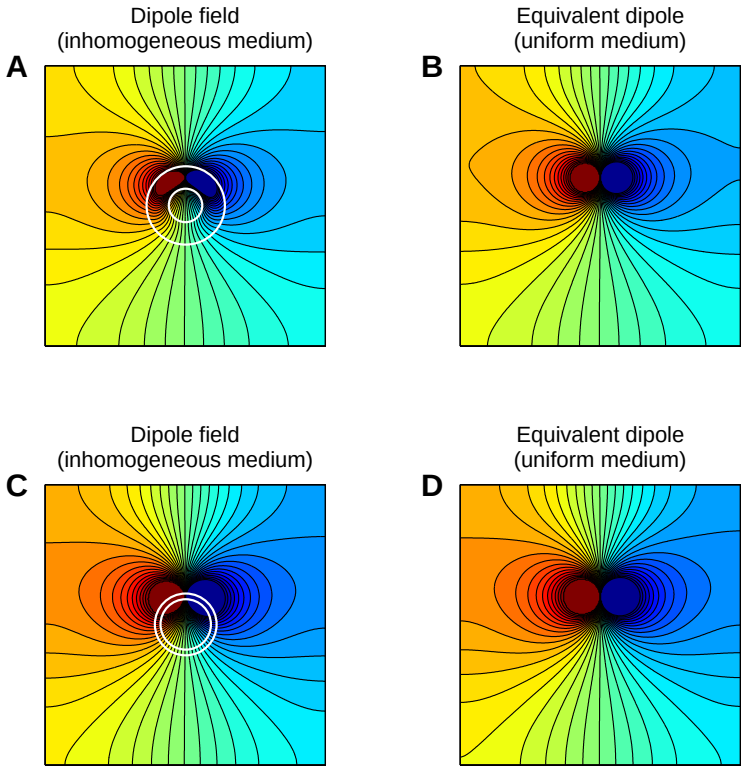

Figure 4: Potential field generated in a 10-by-10 cm volume conductor by a tangent dipole located within an anisotropic annulus with a thickness of 8 mm (A, B) and 2 mm (C, D). The dipole field in the inhomogeneous volume conductor (A, C) is compared to the equivalent dipole in a uniform volume conductor (B, D).

conductor (Fig. 5B,D) was calculated, as well as the field of the corresponding equivalent dipole in a uniform medium (Fig. 5C,E). The results suggest that the equivalent dipole approach is still valid in a thin (3 mm) inhomogeneous tissue.

3.2. Atrial model

The volume conduction problem was solved in a simplified model of the atria in which wall thickness can be controlled. As in the annulus case, the extracellular conductivity within the atrial myocardium was $\sigma_l = 2$ mS/cm (longitudinal, i.e. along

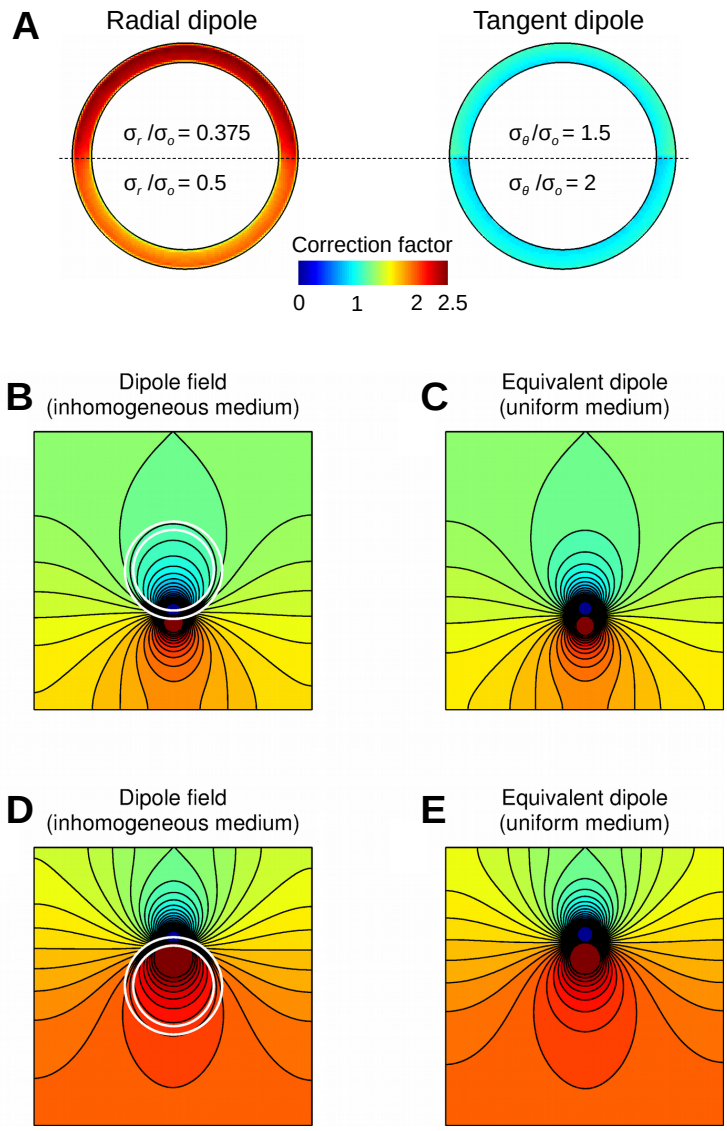

Figure 5: (A) Correction factors M_{rr} (radial) and $M_{\theta\theta}$ (tangent) for annulus with inhomogeneous extracellular conductivity. (B)–(E) Potential field generated in a 10-by-10 cm volume conductor by a radial dipole located within an anisotropic annulus in the lower (B, C) and higher conductivity region (D, E). The dipole field in the inhomogeneous volume conductor (B, D) is compared to the equivalent dipole in a uniform volume conductor (C, E).

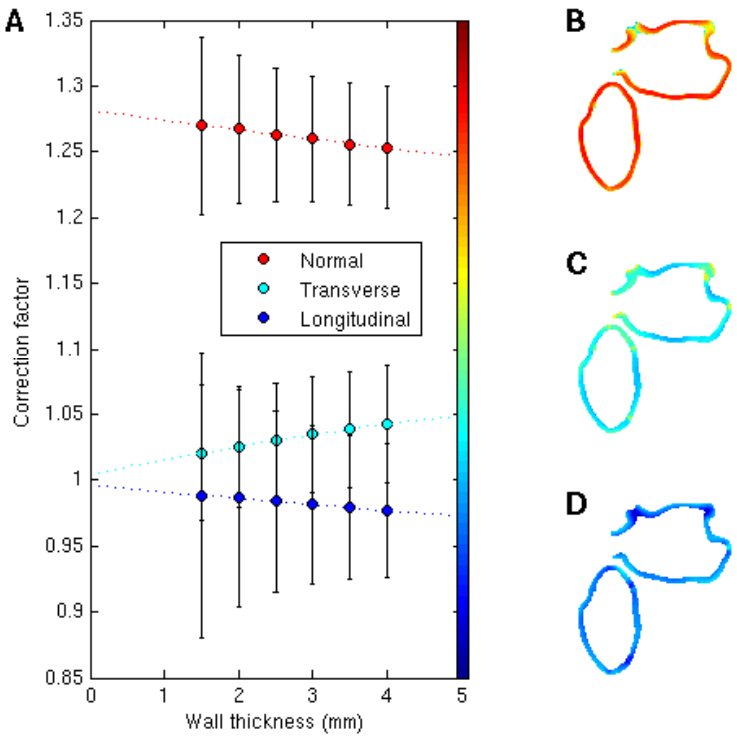

Figure 6: Correction factors M_{ll} (longitudinal), M_{tt} (transverse) and M_{nn} (normal) for atrial geometries of varying wall thicknesses. The mean and standard deviation of the correction factors over the entire atria are shown as error bars (panel A). The spatial distribution of the correction factors is displayed (panel B: normal; C: transverse; D: longitudinal) on a slice of the atria with a thickness set to 3 mm. The color code corresponds to the color bar of panel A. The right atrium is on the bottom-left and the left atrium (including 3 pulmonary veins) on the top.

fiber orientation) and $\sigma_t = \sigma_n = 0.5$ mS/cm (in the transverse direction and that normal to the epicardium). The surrounding bath was isotropic with a conductivity of $\sigma_0 = 1$ mS/cm.

The components of the matrix M was expressed in the local coordinate system (l, t, n) associated with the local fiber orientation. The resulting matrices were nearly diagonal: the off-diagonal components (e.g. M_{lt}, M_{ln},...) were distributed around zero

with a standard deviation of 0.03. The diagonal components are shown in Fig. 6 for a series of models with increasing wall thicknesses. The longitudinal and transverse correction factors M_{ll} and M_{tt} were mostly between 0.95 and 1.05 and tended to 1 as the wall became thinner. The normal correction factors was a bit larger around 1.25. As demonstrated by the standard deviations around 0.05 to 0.1, the correction factors were relatively uniform throughout the atria, as illustrated on Figs. 6B–D, although inhomogeneities in correction factors were still observed, notably in the pulmonary veins. When the size of surrounding bath was extended by 5 mm on all six faces, the difference in terms of correction factors remained very small (of the order of 0.1%), as in the 2D case (Fig. 3).

To evaluate the robustness of the correction factors against changes in geometry and fiber orientation, six left atrial models with a thickness of 2 mm obtained from a former study [21] were used. Figure 7 shows that the resulting correction factors were quantitatively very similar to each other and to the atrial model of Fig. 6 with a 2-mm thickness. The standard deviation of the six mean correction factors of Fig. 7 were 0.0021 (normal), 0.0013 (transverse) and 0.0019 (longitudinal).

3.3. Influence on P waves and F waves

P waves were computed using different sets of correction factors to estimate the effect of that correction on P wave morphology.

First, the same correction factors were applied to the whole tissue. Figure 8 shows that the longitudinal correction factors (M_{ll} from 0.9 to 1.1, $M_{tt} = M_{nn} = 1$) have the largest effect on the P wave. This reflects the fact that current sources are often aligned with fiber direction during sinus rhythm. Note, however, that the estimated values of M_{ll} are around 0.95–1 (Fig. 6), so the actual effect is at least twice smaller. The influence of M_{tt} and M_{nn} were minimal during sinus rhythm.

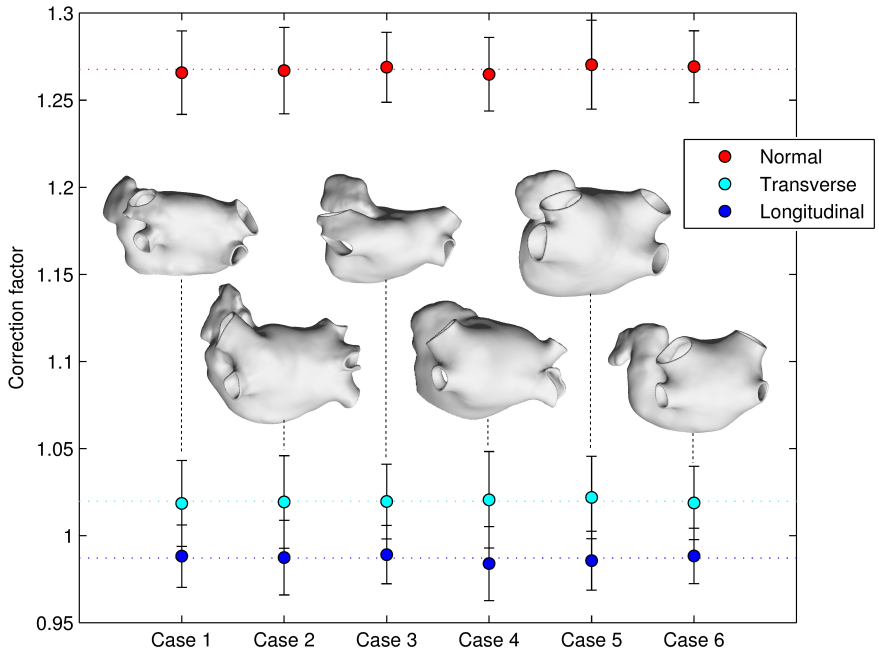

Figure 7: Correction factors M_{ll} (longitudinal), M_{tt} (transverse) and M_{nn} (normal) for different left atrial geometries with a thickness of 2 mm. The mean and standard deviation of the correction factors over the entire atria are shown as error bars for each of the 6 cases.

Then, when all corrections factors were locally optimized using Eq. (4), P wave morphology (black curve in the last row of Fig. 8) remained essentially the same as in the uncorrected case. Global optimization of the correction factors, assuming that they were constant over the whole tissue as in [9], led to the values $M_{ll} = 0.975$, $M_{tt} = 1.045$ and $M_{nn} = 1.273$. The resulting P waves (dashed red curve) were superimposed on the locally-optimized one.

The same procedure was repeated during an episode of simulated atrial fibrillation to assess the influence of varying the activation pattern. The effect of extracellular anisotropy was slightly smaller than during sinus rhythm and was most visible on lead V1, shown on Fig. 9 using the same display format as Fig. 8. Globally-optimized

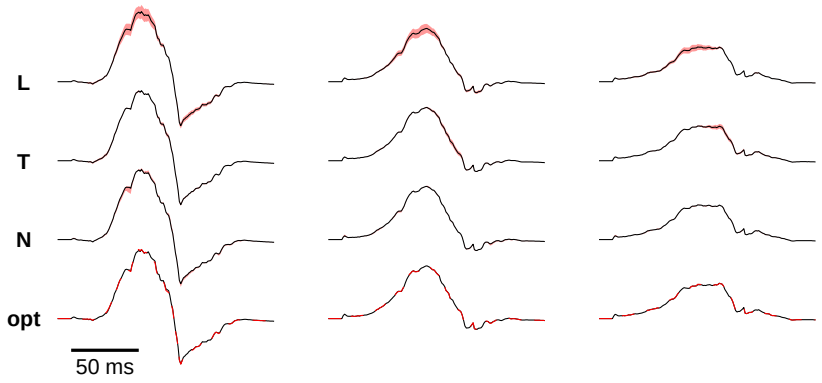

Figure 8: P waves on lead V1, V2 and V3 (from left to right) computed using different sets of correction factors. *First row*: only longitudinal correction factors are applied. The black line corresponds to the non-corrected case $M_{ll} = M_{tt} = M_{nn} = 1$. The red region represents the changes in the P waves when M_{ll} varies from 0.9 to 1.1. *Second row*: M_{tt} is varied from 0.9 to 1.1. *Third row*: M_{nn} is varied from 0.9 to 1.5 (based on Fig. 6, M_{nn} is typically about 1.25). *Fourth row*: P waves computed using locally (black curve) and globally optimized (red curve) correction factors.

correction factors were $M_{ll} = 0.987$, $M_{tt} = 1.033$ and $M_{nn} = 1.181$, within $\approx 1\%$ of those during sinus rhythm, except in the normal direction ($\approx 7\%$ difference).

4. Discussion and conclusion

This study suggests that extracellular myocardial anisotropy in thin-walled tissue (< 3 mm such as in the atria) may be neglected in first approximation when solving the forward problem. In a second approximation, precomputed linear correction factors can be applied to the current sources to improve far-field accuracy (Fig. 4), while using the same boundary element torso model. Small wall thickness was found to be a critical factor to control the effect of extracellular anisotropy. In the thicker-walled ventricles, though, our method would still be applicable [9].

These correction factors tend to slightly reduce dipole source amplitude along fiber

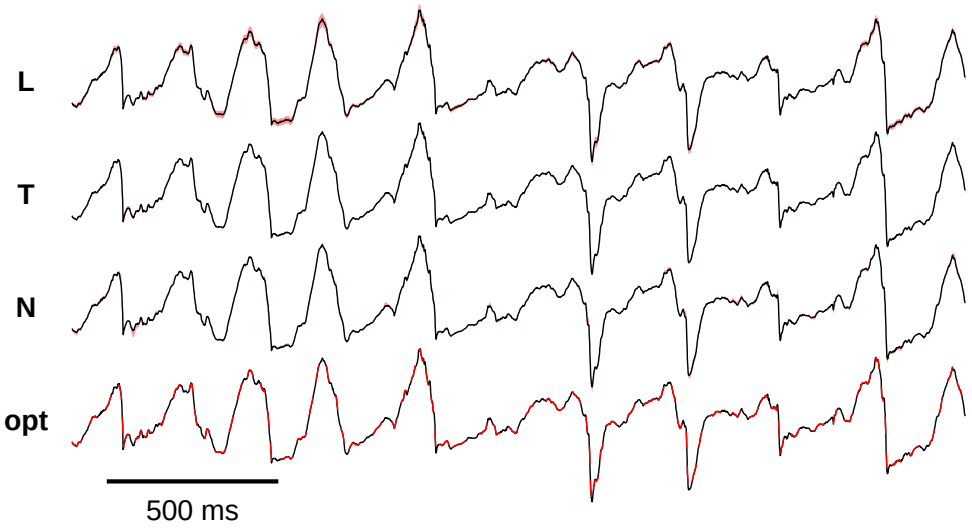

Figure 9: Fibrillatory (F) waves on lead V1 computed using different sets of correction factors during an episode of simulated atrial fibrillation. *First row*: only longitudinal correction factors are applied. The black line corresponds to the non-corrected case $M_{ll} = M_{tt} = M_{nn} = 1$. The red region represents the changes in the F waves when M_{ll} varies from 0.9 to 1.1. *Second row*: M_{tt} is varied from 0.9 to 1.1. *Third row*: M_{nn} is varied from 0.9 to 1.5. *Fourth row*: F waves computed using locally (black curve) and globally optimized (red curve) correction factors.

and slightly increase it in the transverse direction, in agreement with [9]. The correction is stronger in the normal direction corresponding to transmural propagation. Rare in sinus rhythm, breakthroughs may occur (locally) during atrial arrhythmias [22], which advocates for the use of correction factors in these conditions. Nevertheless, transmural correction factors are larger than one only if there is a significant discontinuity in extracellular conductivity when crossing the atrial wall ($\sigma_0 \neq \sigma_t$). The wide range of reported experimental conductivity values [10] makes that statement disputable.

There are several effects of extracellular anisotropy that remain unaffected by the conclusion of our study. First, the conductivity tensor of the monodomain model implicitly or explicitly incorporates information about extracellular anisotropy [11]. Second, extracellular anisotropy in the skeletal muscle or in the ventricular myocardium may be non-negligible [10]. Third, endocardial electrograms may be affected by extracellular anisotropy as well as by blood conductivity. In this latter case, the application of correction factors may help estimate the accuracy of electrogram computation.

Our approach is similar to the lead field theory since it is based on the reciprocity theorem. A difference is that our correction factors do not depend on the lead and not even on the torso volume conductor (e.g. lungs). Another approach would be to compare P waves computed in high-resolution finite element models of the torso with and without atrial extracellular anisotropy, but this would not tell us which components of the dipole sources are most affected.

Despite its lack of flexibility to handle anisotropy directly, the boundary element method has several advantages in terms of mesh creation, computational complexity, solving the inverse problem [23], and computing the contribution of a part of the atria to the ECG (e.g. left and right atria [13]), largely because the body surface potential can be expressed as a transfer matrix applied to the potential in an unbounded uniform medium, a property that was explicitly used in our derivation.

A relatively simple atrial model was used here to make it possible to control atrial wall thickness (outside fast conducting bundles). The same approach can be extended in tissue models with variable thickness and multiple layers with different fiber orientation [24, 25]. However, since the local coordinate system (l, t, n) would vary rapidly in space, the projections of the correction factors (e.g. M_{ll}) would fluctuate so that global scaling of all longitudinal dipole components may not be appropriate. In this case, Eq. (4) would need to be solved at high resolution, but only once, and only in the neighborhood of the atria, not in the full torso. In contrast, the finite element method may require a 3D mesh of the full torso with high resolution within the atrial myocardium, which may be more computationally expensive, although methods have been proposed to provide a good approximation at reduced computational cost [26].

Fully-coupled heart-torso bidomain models have been developed and implemented [27, 28]. When compared to the full bidomain model, the equivalent monodomain model combined with a forward solver proved to be accurate during sinus rhythm both in terms of electrograms [16] and ECG [27]. These results may have to be revisited in models of pathological tissue with strongly unequal anisotropy ratio or when microstructure makes continuous models questionable. In cases where the bioelectric current sources are not accurately described by the monodomain model with an effective conductivity tensor, the equivalent dipole approach proposed here might only be a good approximation to an inappropriate model. This paper only argues that in thin cardiac tissue models, extracellular anisotropy may be neglected or corrected for when solving the Poisson equation for the far-field extracellular potential. The question of whether its feedback on the current sources (i.e. the effect on the propagation equation) can be ignored cannot be answered without a fully-coupled bidomain simulation.

In conclusion, the equivalent dipole approach enables the determination of correction factors that indicate where and how dipole current sources are affected by extracellular

anisotropy. In the thin-walled atria, this effect is shown to have a minor impact on the P wave and thus may be neglected in first approximation.

Acknowledgments

This work was supported by the Natural Sciences and Engineering Research Council of Canada [grant number RGPIN-2015-05658].

References

[1] Y. Rudy, R. Plonsey, A comparison of volume conductor and source geometry effects on body surface and epicardial potentials, Circ Res 46 (2) (1980) 283–91.

[2] R. M. Gulrajani, G. E. Mailloux, A simulation study of the effects of torso inhomogeneities on electrocardiographic potentials, using realistic heart and torso models, Circ Res 52 (1) (1983) 45–56.

[3] P. C. Stanley, T. C. Pilkington, M. N. Morrow, The effects of thoracic inhomogeneities on the relationship between epicardial and torso potentials, IEEE Trans Biomed Eng 33 (3) (1986) 273–84.

[4] S. J. Walker, D. Kilpatrick, Forward and inverse electrocardiographic calculations using resistor network models of the human torso, Circ Res 61 (4) (1987) 504–13.

[5] R. N. Klepfer, C. R. Johnson, R. S. Macleod, The effects of inhomogeneities and anisotropies on electrocardiographic fields: a 3-d finite-element study, IEEE Trans Biomed Eng 44 (8) (1997) 706–19.

[6] C. P. Bradley, A. J. Pullan, P. J. Hunter, Effects of material properties and geometry on electrocardiographic forward simulations, Ann Biomed Eng 28 (7) (2000) 721–41.

[7] P. M. van Dam, A. van Oosterom, Volume conductor effects involved in the genesis of the p wave, Europace 7 (s2) (2005) S30–S38.

[8] R. Modre, M. Seger, G. Fischer, C. Hintermuller, D. Hayn, B. Pfeifer, F. Hanser, G. Schreier, B. Tilg, Cardiac anisotropy: is it negligible regarding noninvasive activation time imaging?, IEEE Trans Biomed Eng 53 (4) (2006) 569–80.

[9] M. Potse, B. Dubé, A. Vinet, Cardiac anisotropy in boundary-element models for the electrocardiogram, Medical & biological engineering & computing 47 (7) (2009) 719–729.

[10] D. U. Keller, F. M. Weber, G. Seemann, O. Dossel, Ranking the influence of tissue conductivities on forward-calculated ecgs, Biomedical Engineering, IEEE Transactions on 57 (7) (2010) 1568–1576.

[11] R. M. Gulrajani, Bioelectricity and biomagnetism, New York: Wiley, 1998.

[12] V. Jacquemet, A. van Oosterom, J.-M. Vesin, L. Kappenberger, Analysis of electrocardiograms during atrial fibrillation. a biophysical model approach, IEEE Eng Med Biol Mag 25 (6) (2006) 79–88.

[13] V. Jacquemet, Modeling left and right atrial contributions to the ecg: A dipole-current source approach, Comput Biol Med 65 (2015) 192–9.

[14] V. Jacquemet, N. Virag, Z. Ihara, L. Dang, O. Blanc, S. Zozor, J.-M. Vesin, L. Kappenberger, C. Henriquez, Study of unipolar electrogram morphology in a computer model of atrial fibrillation, J Cardiovasc Electrophysiol 14 (10 Suppl) (2003) S172–9.

[15] C. S. Henriquez, N. Trayanova, R. Plonsey, A planar slab bidomain model for cardiac tissue, Ann Biomed Eng 18 (4) (1990) 367–76.

[16] J. V. Tranquillo, D. O. Burwell, C. S. Henriquez, Analytical model of extracellular potentials in a tissue slab with a finite bath, IEEE Trans Biomed Eng 52 (2) (2005) 334–8.

[17] D. Gabor, N. C. V, The determination of the resultant dipole of the heart from measurements on the body surface, J Appl Phys 25 (1956) 413.

[18] A. van Oosterom, Z. Ihara, V. Jacquemet, R. Hoekema, Vectorcardiographic lead systems for the characterization of atrial fibrillation, J Electrocardiol 40 (4) (2007) 343.e1–11.

[19] G. T. Buzzard, J. J. Fox, F. Siso-Nadal, Sharp interface and voltage conservation in the phase field method: application to cardiac electrophysiology, SIAM Journal on Scientific Computing 30 (2) (2008) 837–854.

[20] N. Virag, V. Jacquemet, L. Kappenberger, Modeling of atrial fibrillation, in: Cardiac Mapping, Fourth Edition, Wiley Online Library, 2012, pp. 131–139.

[21] A. Herlin, V. Jacquemet, Eikonal-based initiation of fibrillatory activity in thin-walled cardiac propagation models, Chaos 21 (4) (2011) 043136.

[22] A. Gharaviri, S. Verheule, J. Eckstein, M. Potse, N. H. Kuijpers, U. Schotten, A computer model of endo-epicardial electrical dissociation and transmural conduction during atrial fibrillation, Europace 14 (suppl 5) (2012) v10–v16.

[23] A. van Oosterom, V. Jacquemet, Genesis of the p wave: atrial signals as generated by the equivalent double layer source model, Europace 7 (s2) (2005) S21–S29.

[24] M. W. Krueger, V. Schmidt, C. Tobón, F. M. Weber, C. Lorenz, D. U. Keller, H. Barschdorf, M. Burdumy, P. Neher, G. Plank, et al., Modeling atrial fiber

orientation in patient-specific geometries: a semi-automatic rule-based approach, in: Functional imaging and modeling of the heart, Springer, 2011, pp. 223–232.

[25] F. Pashakhanloo, D. A. Herzka, H. Ashikaga, S. Mori, N. Gai, D. A. Bluemke, N. A. Trayanova, E. R. McVeigh, Myofiber architecture of the human atria as revealed by submillimeter diffusion tensor imaging, Circ Arrhythm Electrophysiol 9 (4) (2016) e004133.

[26] M. J. Bishop, G. Plank, Bidomain ECG simulations using an augmented monodomain model for the cardiac source, IEEE Trans Biomed Eng 58 (8) (2011) 2297–2307.

[27] M. Potse, B. Dubé, J. Richer, A. Vinet, R. M. Gulrajani, A comparison of monodomain and bidomain reaction-diffusion models for action potential propagation in the human heart, IEEE Trans Biomed Eng 53 (12) (2006) 2425–2435.

[28] L. Cardone-Noott, A. Bueno-Orovio, A. Mincholé, N. Zemzemi, B. Rodriguez, Human ventricular activation sequence and the simulation of the electrocardiographic QRS complex and its variability in healthy and intraventricular block conditions, Europace 18 (suppl 4) (2016) iv4–iv15.